# A 2-DV NUMERICAL SOLUTION FOR THE TURBULENT WAVE BOUNDARY LAYER UNDER BREAKING WAVES

Nguyen The Duy[1], Tomoya Shibayama[2] and Akio Okayasu[3]

## Abstract

*This paper presents a numerical solution for the bottom boundary layer (BBL) in the surf zone. The upper boundary of the BBL is determined through the solution of a breaking waves model. Different turbulence models have been tested to determine the distribution of turbulent kinetic energy, energy dissipation and eddy viscosity in the BBL. Finally, the vertical profiles of horizontal velocity can be found out through the solution of the governing equations of the BBL.*

## Introduction

A quantitative study of the hydrodynamics of the bottom boundary layer (BBL) is necessary for determining precisely the near-bottom shear stress, a major driving force in predicting the transport of sediment in coastal areas. Various studies on the mechanics of the wave boundary layers under non-breaking condition have been reported in the literature (e.g. Kajura 1968, Kamphuis 1975, Grant and Madsen 1979, Trowbridge and Madsen 1984, Larson 1995, etc.). Under breaking waves, however, development in the study of the BBL has been limited because of the following unsolved or unsatisfactorily solved problems.

(1) The free stream velocity at the upper edge of the BBL, an important boundary for solving BBL flow, still cannot be determined properly by available 1-D or 2-DH breaking wave models. Outside the BBL, it is necessary to solve a 2-DV breaking wave model in order to determine directly the upper boundary condition of the BBL from computed vertical profile of water particle velocity. For this purpose, the breaking waves model presented by Duy et al. (1996), Duy and Shibayama (1997) has been applied in the present study.

(2) The effect of turbulence induced by waves breaking on the turbulence structure of the BBL is still not understood adequately. In this study, it is assumed that in

[1] Dr. Eng., Dept. of Civil Eng., Ho Chi Minh University of Technology, 268 Ly Thuong Kiet, Q.10, Ho Chi Minh City, Vietnam.

[2] Dr. Eng., Professor, Dept. of Civil Eng., Yokohama National University, Hodogaya-ku, Yokohama 240, Japan.

[3] Dr. Eng., Assoc. Prof., Dept. of Civil Eng., Yokohama National University, Hodogaya-ku, Yokohama 240, Japan.

case of a surf zoue formed by spilling breakers, the transfer of turbulence from the upper layer to the BBL is negligible and therefore the turbulence production resulted from shear is dominant in the BBL.

(3) The lack of reliable measured velocity data that cau be used for verifying a BBL model in the surf zone.

## Model formulation

At each time level of computation, a three-step procedure is utilized to solve the 2-DV flow equations for the BBL. This solution procedure is illustrated in the flow diagram below.

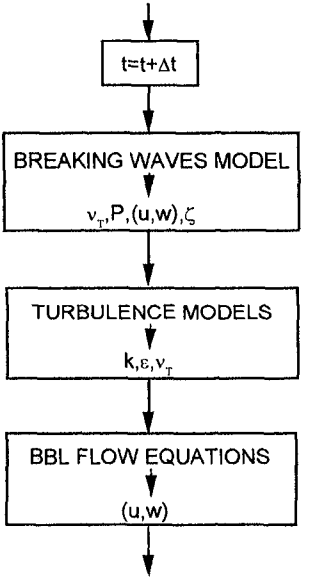


Figure 1. Flow diagram of solution procedure.

- In the first step, the breaking waves model is solved for the water domain outside the BBL (the upper layer) to determine the wave variables in 2-DV plane such as water surface, pressure field and velocity field. The result of this solution provides the values of velocity vectors at the upper boundary of the BBL.
- In the second step, turbulence structure of the BBL is iuvestigated through the solution and comparison of the following turbulence models: eddy viscosity model, $k$-model and $k\varepsilon$-model. From this solution, it is possible to find out the distribution of eddy viscosity, turbulent kinetic energy and energy dissipation inside the BBL.
- In the final step, the results obtained from the previous two steps are used as input data to solve the governing equations for the BBL. From which, the velocity field in the BBL can be determined.

The governing equations and boundary conditions used in the second and third step of the solution procedure are described briefly as follows.

In a 2-DV plane, the flow in the BBL can be modeled by the following equations

$$\frac{\partial u}{\partial x}+\frac{\partial w}{\partial z}=0 \tag{1}$$

$$\frac{\partial u}{\partial t}+u\frac{\partial u}{\partial x}+w\frac{\partial u}{\partial z}-\frac{1}{\rho}\frac{\partial \tau_{zx}}{\partial z}=\frac{\partial u_e}{\partial t}+u_e\frac{\partial u_e}{\partial x} \tag{2}$$

where ($u$, $w$): Reynolds-averaged velocity vector; $\tau_{zx}$: Reynolds shear stress; $u_e$: free stream velocity. The momentum term due to turbulent motion can be expressed as

$$\frac{1}{\rho}\frac{\partial \tau_{zx}}{\partial z}=\nu_T\frac{\partial}{\partial z}\left(\nu_T\frac{\partial u}{\partial z}\right) \tag{3}$$

In (2), the momentum terms on the right hand side are the forcing function reflecting the process of water motion in the region outside the BBL. Along the edge of the BBL, these momentum terms can be determined by using the 2-DV turbulent flow model for breaking waves developed by Duy et al. (1996).

The boundary conditions for the BBL equations are introduced in the following.

$$u=0,\ w=0 \quad \text{for} \quad z=0 \tag{4}$$

$$u\to u_e,\ w\to w_e \quad \text{for} \quad z\to\infty \tag{5}$$

and at the seaward and shoreward boundary (side boundaries), a logarithmic distribution is assumed for the vertical profile of horizontal velocity in the BBL

$$u=u_e\ln\left(C_1z+C_2\right) \quad \text{for} \quad x=0 \text{ or } x=x_{\max} \tag{6}$$

in which the constants $C_1$ and $C_2$ are determined by using the boundary conditions (4) and (5)

$$C_1=\frac{e-1}{\delta} \tag{7}$$

$$C_2=1 \tag{8}$$

where $\delta$ is the thickness of the BBL and $e$ the natural logarithmic base.

At the side boundaries, the vertical velocities are determined by substituting Eq. (6) into the mass conservation, Eq. (1), and then solve for $w$.

In addition to the above boundary conditions, it is necessary to know the distribution of the eddy viscosity in the BBL to solve (1) and (2). Three different solutions of the eddy viscosity are investigated in the present study.

In the first solution, the following equation of the eddy viscosity, or also known as the eddy viscosity model, is applied for the entire boundary layer thickness (e.g., Kajura 1968, Grant and Madsen 1979)

$$\nu_T=\kappa u_* z \tag{9}$$

where $\kappa$ is the Karman constant ($\kappa$=0.4), $z$ the vertical elevation from the bottom and $u_*$ the friction velocity

$$u_*=\sqrt{0.5f_w u_{em}^2} \tag{10}$$

where $f_w$ is the wave friction factor and $u_{cm}$ the maximum horizontal velocity at the upper boundary of the BBL. Eq. (10) expresses a linear distribution of the eddy viscosity inside the BBL. In fact, this time-invariant eddy viscosity has been originally developed to simulate non-breaking wave boundary layers.

The second solution of the eddy viscosity is based on the transport equation for turbulent kinetic energy, or the *k*-equation, which in a 2DV-plane reads

$$\frac{dk}{dt} = \frac{\partial}{\partial x}\left(\frac{\nu_T}{\sigma_k}\frac{\partial k}{\partial x}\right) + \frac{\partial}{\partial z}\left(\frac{\nu_T}{\sigma_k}\frac{\partial k}{\partial z}\right) + \frac{PROD}{\rho} - c_2\frac{k^{3/2}}{l_d} \tag{11}$$

in which

$$\frac{dk}{dt} = \frac{\partial k}{\partial t} + \frac{\partial (uk)}{\partial x} + \frac{\partial (wk)}{\partial z} \tag{12}$$

PROD is the turbulence production, $c_2$ a constant, and $l_d$ the length scale of turbulence

$$l_d = \kappa \sqrt[4]{c_2}\, z \tag{13}$$

In the *k*-equation, the eddy viscosity is determined by the following expression

$$\nu_T = l_d \sqrt{k} \tag{14}$$

Under breaking waves condition, the turbulence production in the BBL can be assumed to be resulted from two different sources: one is the transfer of breaker-generated turbulence from the upper layer to the BBL, denoted by *TRANS*, and one is caused by shear inside the BBL.

$$PROD = TRANS + \rho \nu_T \left(\frac{\partial u}{\partial z}\right)^2 \tag{15}$$

In case of spilling breakers, as mentioned above, it may be reasonable to assume that

$$TRANS \to 0 \quad \text{for} \quad z \to 0 \tag{16}$$

Therefore, the turbulence production resulted from shear is dominant in the BBL, and Eq. (15) becomes

$$PROD = \rho \nu_T \left(\frac{\partial u}{\partial z}\right)^2 \tag{17}$$

The boundary conditions for the *k*-equation are

$$k = \frac{1}{\sqrt{c_2}} \nu_T \frac{\partial u}{\partial z} \quad \text{for} \quad z = \frac{k_N}{30} \tag{18}$$

and

$$\frac{\partial k}{\partial z} = 0 \quad \text{for} \quad z \to \infty \tag{19}$$

in which $k_N$ is the bed roughness.

Eq. (18) is derived by assuming that there is local equilibrium between production and dissipation close to the bottom. Eq. (19) is based on the assumption (16), i.e. there is no flux of turbulent kinetic energy at the upper boundary.

At the side boundaries, a uniform distribution of turbulent kinetic energy in the $x$-direction is assumed.

The third solution of the eddy viscosity is based on the transport equations for turbulent kinetic energy and dissipation, or the $k\varepsilon$-equations, which in a 2DV-plane reads

$$\frac{dk}{dt} = \frac{\partial}{\partial x}\left(\frac{\nu_T}{\sigma_k}\frac{\partial k}{\partial x}\right) + \frac{\partial}{\partial z}\left(\frac{\nu_T}{\sigma_k}\frac{\partial k}{\partial z}\right) + \nu_T\left(\frac{\partial u}{\partial z}\right)^2 - \varepsilon \tag{20}$$

$$\frac{d\varepsilon}{dt} = \frac{\partial}{\partial x}\left(\frac{\nu_T}{\sigma_\varepsilon}\frac{\partial \varepsilon}{\partial x}\right) + \frac{\partial}{\partial z}\left(\frac{\nu_T}{\sigma_\varepsilon}\frac{\partial \varepsilon}{\partial z}\right) + c_{1\varepsilon}\varepsilon\frac{\nu_T}{k}\left(\frac{\partial u}{\partial z}\right)^2 - c_{2\varepsilon}\frac{\varepsilon^2}{k} \tag{21}$$

$$\nu_T = c_\mu \frac{k^2}{\varepsilon} \tag{22}$$

where $\sigma_k$, $\sigma_\varepsilon$, $c_{1\varepsilon}$, $c_{2\varepsilon}$ and $c_\mu$ are empirical constants.

The boundary conditions for the $k\varepsilon$-equations are

$$k = \frac{1}{\sqrt{c_2}}\nu_T\frac{\partial u}{\partial z} \quad \text{for} \quad z = \frac{k_N}{30} \tag{23}$$

$$\frac{\partial k}{\partial z} = 0 \quad \text{for} \quad z \to \infty \tag{24}$$

$$\varepsilon = (c_2)^{3/4}\frac{k^{3/2}}{\kappa z} \quad \text{for} \quad z = \frac{k_N}{30} \tag{25}$$

$$\frac{\partial \varepsilon}{\partial z} = 0 \quad \text{for} \quad z \to \infty \tag{26}$$

And similar to the $k$-equation, uniform distributions of $k$ and $\varepsilon$ in the $x$-direction are also assumed at the side boundaries.

In the second and third step of the solution procedure (Figure 1), the governing equations and corresponding boundary conditions are solved by the finite difference method, using a fully implicit scheme. On a sloping bottom, in order to establish a linear numerical mesh in which the grid lines are parallel to the coordinates axes, the $(x,z)$ domain is transformed to the $(\xi,\eta)$ domain as shown in Figure 2.

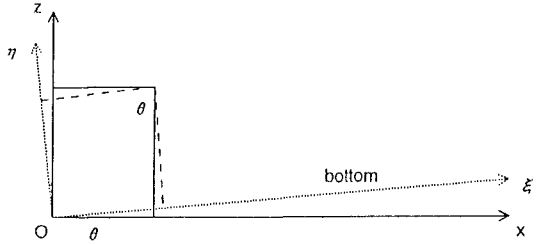


Figure 2. Coordinates transformation for numerical solution.

The functional relationship between the $(x,z)$ and $(\xi,\eta)$ coordinates systems is expressed by

$$x = \xi \cos\theta - \eta \sin\theta \tag{27}$$

$$z = \xi \sin\theta + \eta \cos\theta \tag{28}$$

From (27) and (28), the Jacobian matrix of the transformation can be determined as follows

$$J = \begin{bmatrix} \frac{\partial \xi}{\partial x} & \frac{\partial \xi}{\partial z} \\ \frac{\partial \eta}{\partial x} & \frac{\partial \eta}{\partial z} \end{bmatrix} = \begin{bmatrix} \cos\theta & \sin\theta \\ -\sin\theta & \cos\theta \end{bmatrix} \tag{29}$$

The first derivatives of the velocity components in the computational domain are then determined by the chain rule, using the Jacobian matrix (29)

$$\begin{bmatrix} \frac{\partial u}{\partial x} & \frac{\partial u}{\partial z} \\ \frac{\partial w}{\partial x} & \frac{\partial w}{\partial z} \end{bmatrix} = \begin{bmatrix} \frac{\partial u}{\partial \xi} & \frac{\partial u}{\partial \eta} \\ \frac{\partial w}{\partial \xi} & \frac{\partial w}{\partial \eta} \end{bmatrix} \begin{bmatrix} \frac{\partial \xi}{\partial x} & \frac{\partial \xi}{\partial z} \\ \frac{\partial \eta}{\partial x} & \frac{\partial \eta}{\partial z} \end{bmatrix} \tag{30}$$

while the time derivative ($\partial/\partial t$) remains unchanged in the transfomed domain.

## Numerical results

Some numerical results of the present model are compared with the laboratory data of Cox et al. (1996). In this experiment, an extensively detailed measurement of surf zone hydrodynamics was reported for the case of a spilling breaker. The velocity profiles were measured at different locations in a surf zone by using a laser-Doppler velocimeter. At each location, 30 measuring points were set along the verical line, of which 10 points were located in the near-bottom area. In the experiment, the wave period was 2.2 s, the water depth in the constant depth section was 0.4 m, and the wave height was 17.10 cm at breaking. The 1:35 bottom slope was filled with natural sand of 1.0 mm median grain diameter. The boundary layer thickness was found to be appoximately 1 cm in this experiment.

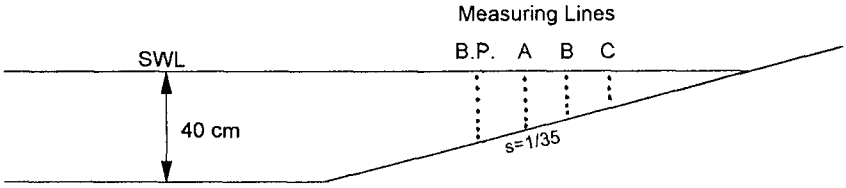


Figure 3. Locations of measuring lines in the surf zone.

In Figure 3, according to the experimental observation, section A is in the transition region where the wave form goes from organized motion to a turbulent bore; and sections B and C are in the inner surf zone where the saw-toothed wave shape is a well-developed turbulent bore.

Figure 4 shows a result obtained in the first step of the solution procedure (Figure 1), that is the time series of horizontal velocity at different positions outside the BBL which are computed by the breaking waves model of Duy et al. (1996). In this figure, the variable $X$ denotes horizontal distance from the shoreline of the still water, subscript "b" denotes the breaking point, and $z$ is the vertical elevation from the

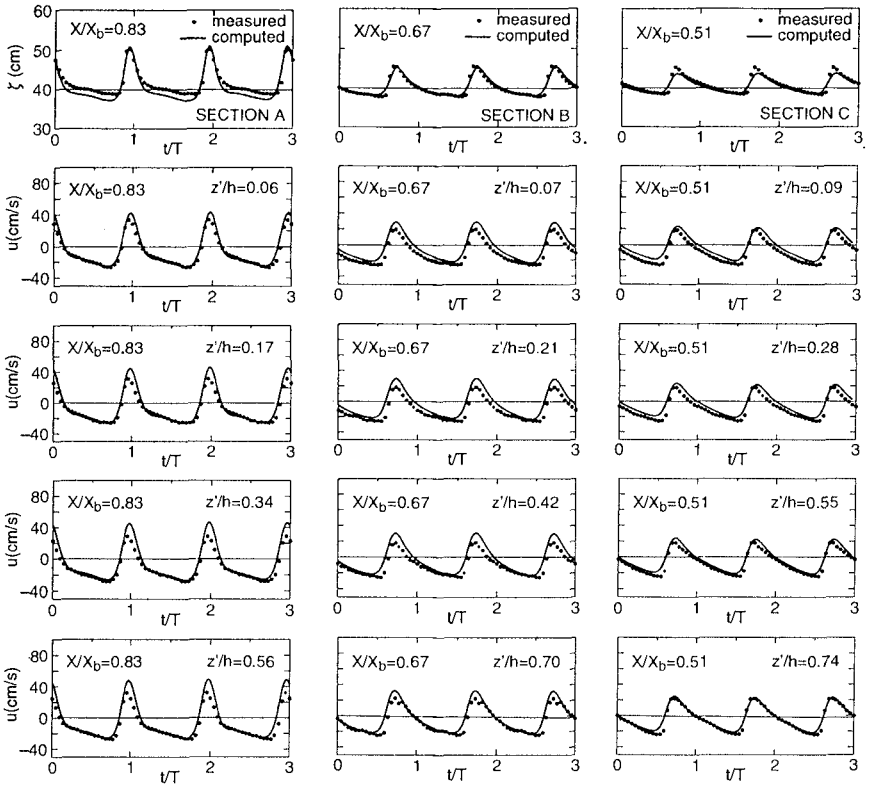


Figure 4. Time series of water surface elevation $\zeta$ and horizontal velocity $u$.

bottom. The comparisons show that the model is capable of simulating the deformation of the velocity profiles as wave propagates shoreward and of producing the high nonlinearity of the velocity profiles in shallow water area. As a general tendency, in the transition region (section A), the model results overestimate the peak values of horizontal velocity at elevations far away from the bottom. At sections in the inner surf zone (sections B and C), reasonable agreements are obtained between the simulated and measured velocities.

In the second step of computational procedure, the turbulence structure of the BBL is examined through the solutions of different turbulence models.

Figure 5 presents the water surface computed by the breaking waves model and the distribution of turbulent kinetic energy in the BBL computed by the $k$-equation. The wave decay due to energy dissipation in the surf zone can be observed from the surface elevations at different phases. At each phase, it can be seen that the developing cores of $k$ are originated from the bottom and correspond to the locations of wave crests at the water surface. And as wave moves shoreward, the magnitude of $k$ decreases gradually. This distribution pattern of $k$ may be caused by the following: (1) the assumption that turbulence production resulted from shear is dominant in the BBL, and

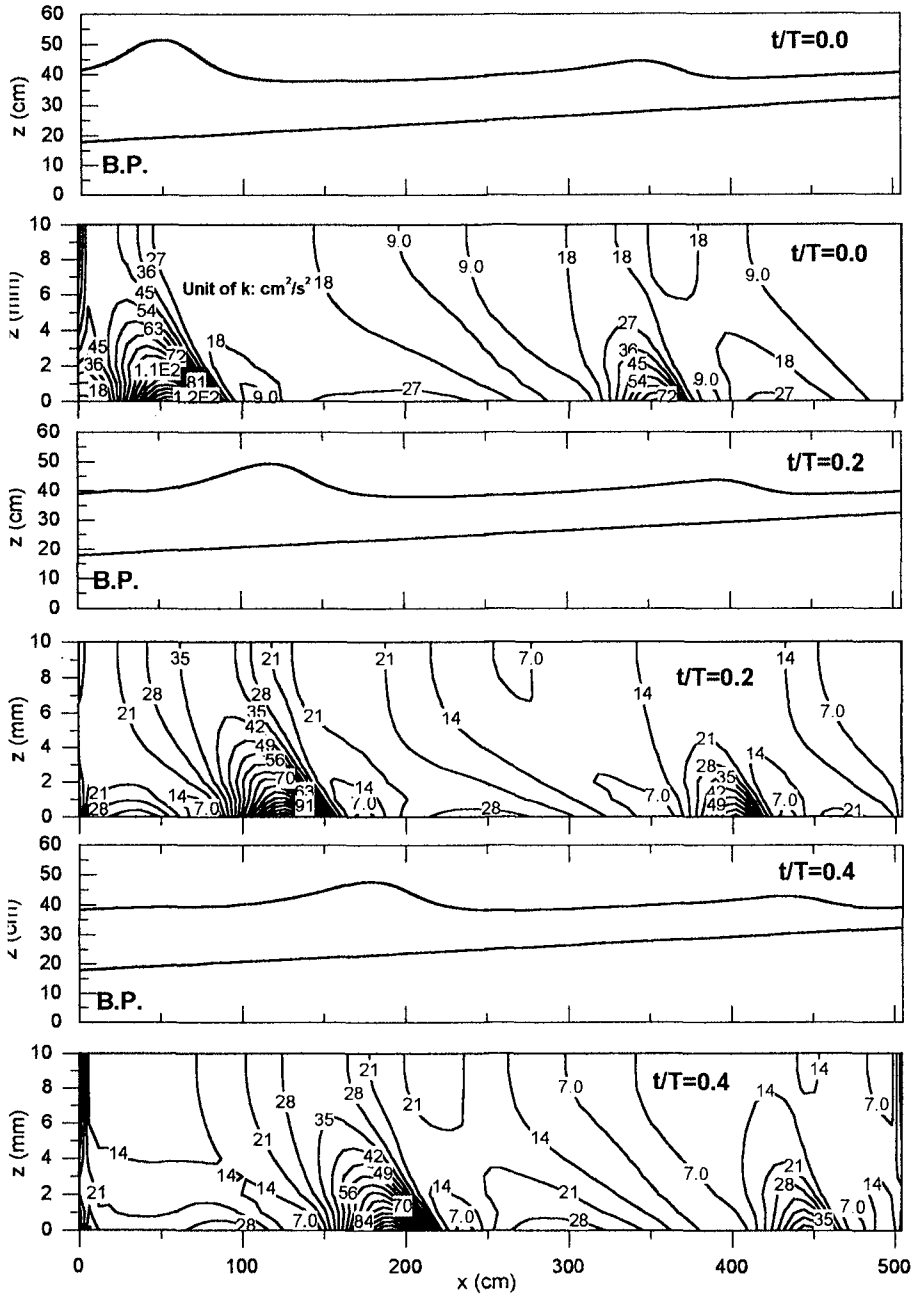


Figure 5. Distribution of turbulent kinetic energy in the bottom boundary layer in a surf zone (solution of the $k$ - equation )

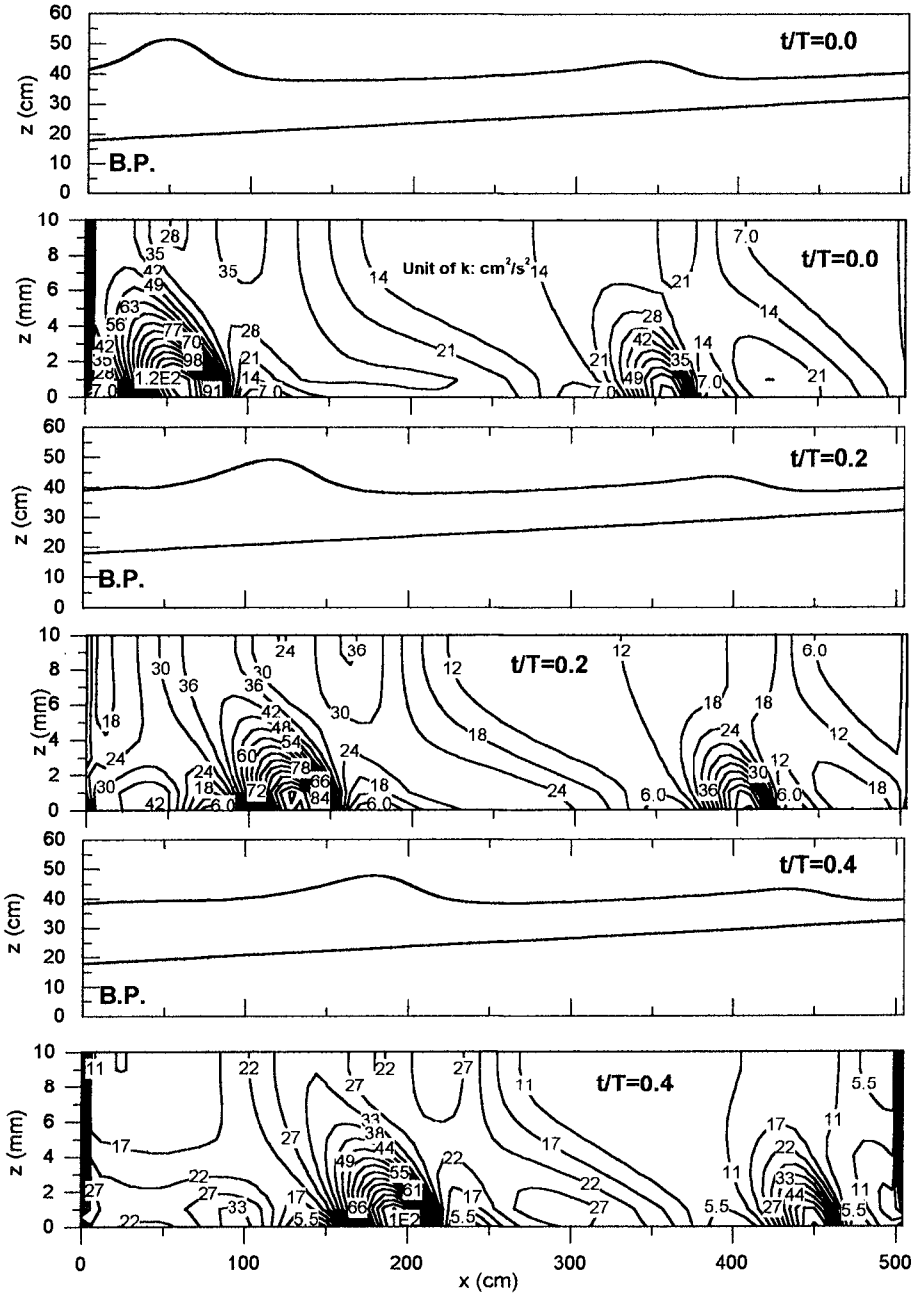


Figure 6. Distribution of turbulent kinetic energy in the bottom boundary layer in a surf zone (solution of the $k\varepsilon$-equations).

(2) the effect of the upper boundary, which is expressed by the forcing function on the right hand side of Equation (2).

Figure 6 also presents the distribution of turbulent kinetic energy in the BBL for different phases, but from the solution of the $k\varepsilon$ - equations. Very similar distributions of $k$ can be seen for the solutions of the $k$-equation and the $k\varepsilon$ - equations. Quantitatively, the differences in $k$ magnitude between the above two models are less than 5%.

The numerical results of turbulent kinetic energy are compared with laboratory data as shown in Figure 7. The time series of $k$ at different positions in the BBL again indicate that the results of the $k$-equation and the $k\varepsilon$ - equations are very similar. The comparison with laboratory data shows that the agreement between computed and measured values is not good around the peak of $k$. At other phases of the wave period, reasonable agreements are obtained.

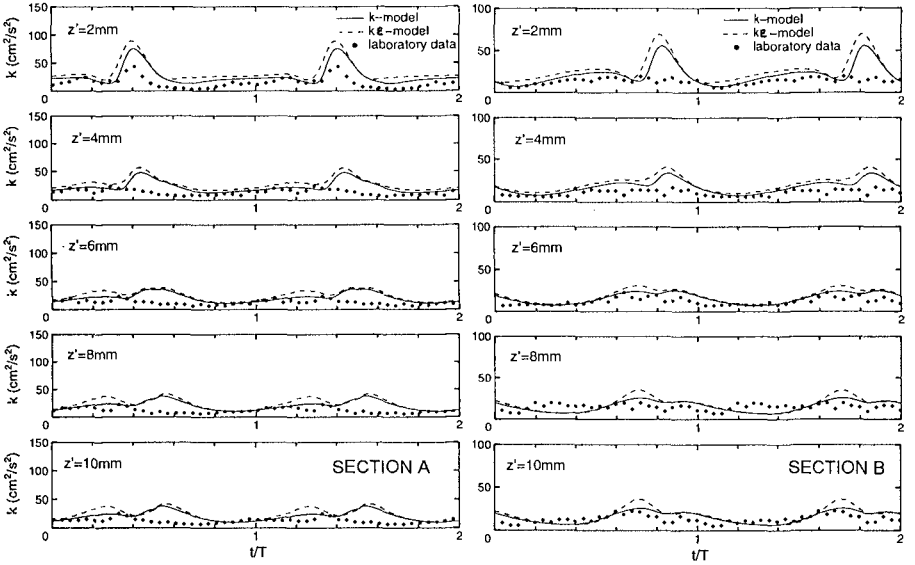


Figure 7. Time series of turbulent kinetic energy in the bottom boundary layer.

Figure 8 also plots a result of the $k\varepsilon$ - equations, that is the distribution of energy dissipation, $\varepsilon$, in the BBL. Similarly to the distribution of $k$, zones of large energy dissipation are also originated from the bottom and correspond to the locations of wave crests at the water surface. This means that large dissipation occurs where there exists high turbulent kinetic energy. The magnitude of energy dissipation is smaller at locations closer to the shoreline. With known distributions of $k$ and $\varepsilon$, the distribution of eddy viscosity in the BBL can be determined as shown in Figure 9.

With known distribution of the eddy viscosity, Equations (1) and (2) can be solved to determine the velocity field in the BBL. Figure 10 presents the computed vertical profiles of horizontal velocities inside the BBL corresponding to different distributions of the eddy viscosity. There are certain differences between these three velocity profiles. However, they exhibit the similar features as follows: (1) when the flow

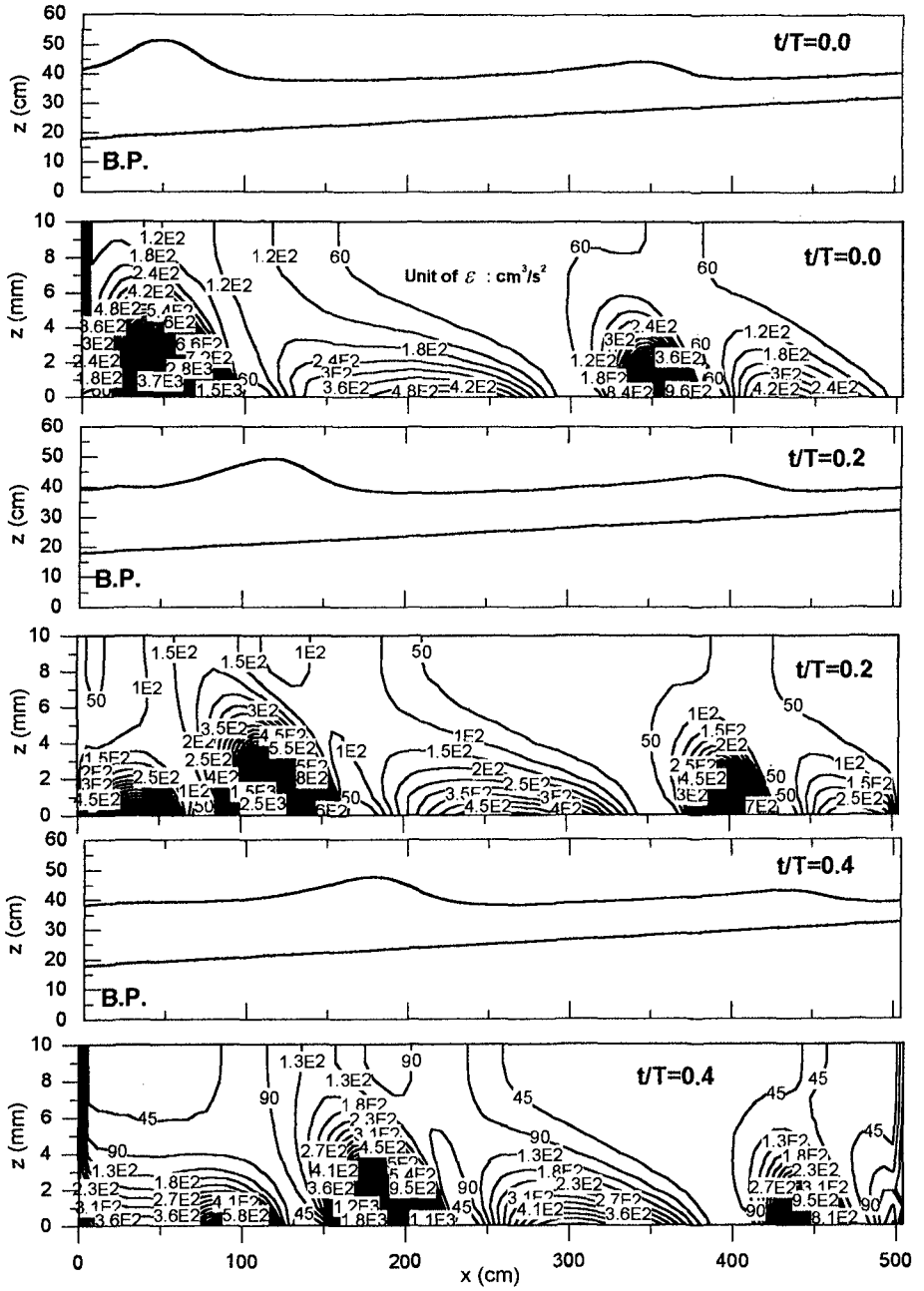


Figure 8. Distribution of energy dissipation in the bottom boundary layer in a surf zone (solution of the $k\varepsilon$-equations).

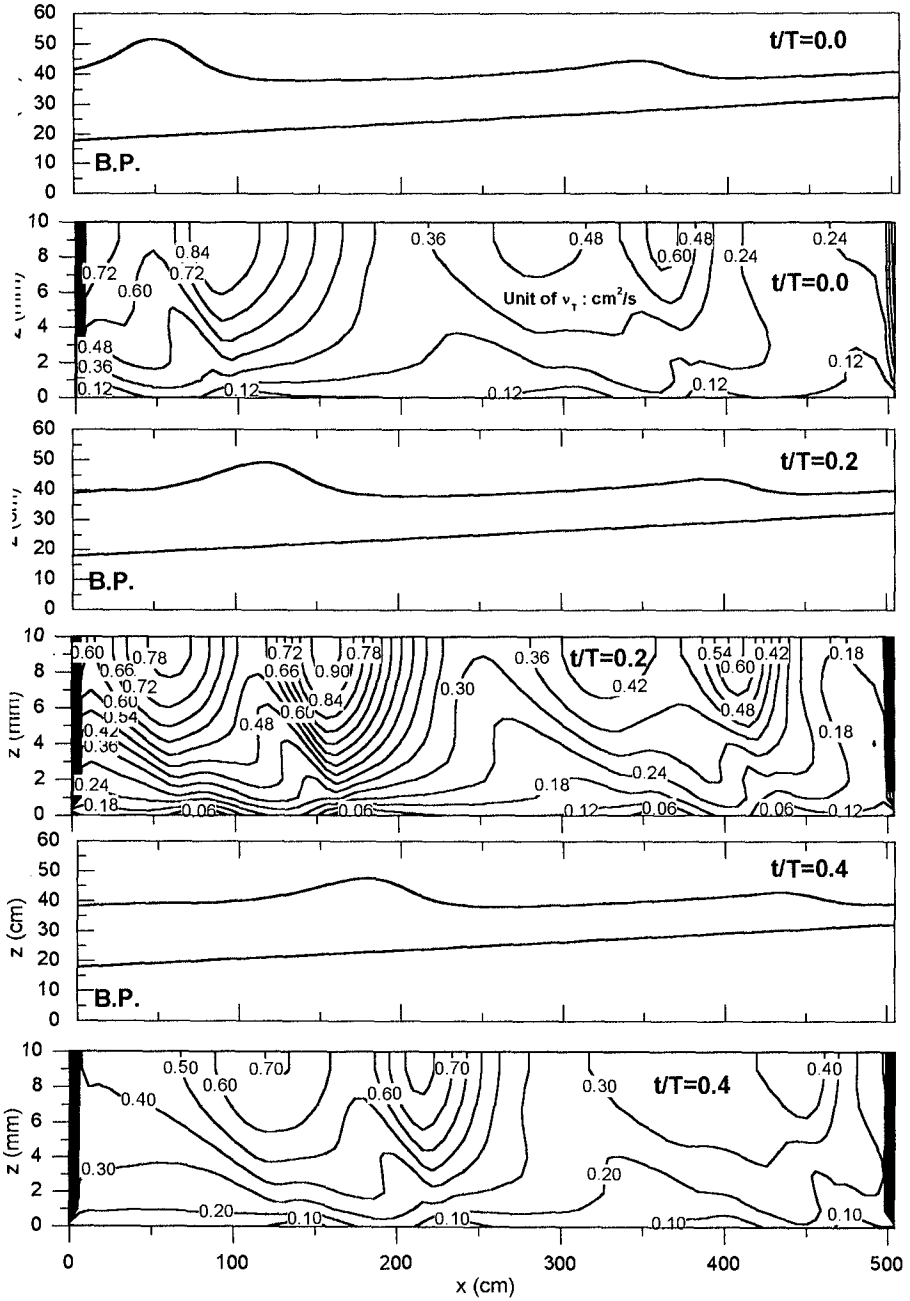


Figure 9. Distribution of eddy viscosity in the bottom boundary layer in a surf zone (solution of the $k\varepsilon$ - equations)

changes direction, the near-bottom velocity always turns before the free stream velocity, both in the increasing and the decreasing stages of the water surface; this indicates a phase difference between the near-bottom velocity and the free stream velocity, a typical feature of oscillatory boundary layers that has been also observed for non-breaking waves, (2) as a result of the nonlinearity and asymmetry of the time variation of the water surface and the free stream velocity in the surf zone, the velocity amplitude of the shoreward flow is larger than that of the seaward flow, and (3) the velocity amplitude is largest at certain elevation inside the BBL, not at the upper edge of the layer. The comparison with laboratory data show that the numerical model is capable of predicting reasonably the velocity profiles inside the boundary layer for most phases of the wave period. However, at the phases when the velocities of the seaward flow reach their maximum values, the slope of the measured velocity profile at the area very close to the bottom tends to decrease and the present model fails to predict such change.

For the specific comparison shown in Figure 10, the calculation of the standard deviations indicates that when solving equations (1) and (2) with the eddy viscosity computed by the $k$-model, best agreement is obtained between the simulated velocity profiles and laboratory data.

## Conclusions

Under breaking waves condition, the flow inside the BBL was modeled by solving numerically the 2-DV governing equations for the bottom boundary layer for the entire surf zone. The comparisons with laboratory data show that the numerical model is capable of predicting reasonably the distribution of turbulent kinetic energy as well as the velocity profiles inside the boundary layer for most phases of the wave period.

## References

Duy, N.T., T. Shibayama, and A. Okayasu, A 2-DV numerical solution for the turbulent wave boundary layer under breaking waves, in *Book of Abs. of 26th Coastal Engineering Conference,* 550-551, ASCE, Copenhagen, 1998.

Duy, N.T. and T. Shibayama , A convection-diffusion model for suspended sediment in the surf zone, *J. of Geophys. Res., 102* (C10), 23169-23186, 1997.

Duy, N.T., T. Shibayama, and A. Okayasu, A turbulent flow model for breaking waves, in *Proceedings of 25th Coastal Engineering Conference,* 200-212, ASCE, Orlando, 1996.

Cox, D.T., N. Kobayashi, and A. Okayasu, Experimental and numerical modeling of surf zone hydrodynamics, *Res. Report No. CACR-95-07,* Center for Applied Coastal Res., Univ. of Delaware, 1996.

Grant, W.D. and O.S. Madsen, Combined wave and current interaction with a rough bottom, *J. of Geophys. Res., 84*(C4), 1797-1808, 1979.

Kajura, K., A model of the bottom boundary layer in water waves, *Bull. Earthquake Res. Inst., 46,* 75-123, 1968.

Larson, M., Closed-form solution of turbulent wave boundary layer, *Proc. of Coastal Eng., JSCE, 42*(1), 26-30, 1995.

Trowbridge, J. and O.S. Madsen, Turbulent wave boundary layers, 1, Model formulation and first-order solution, *J. of Geophys. Res., 89*(C5), 7989-7997, 1984.

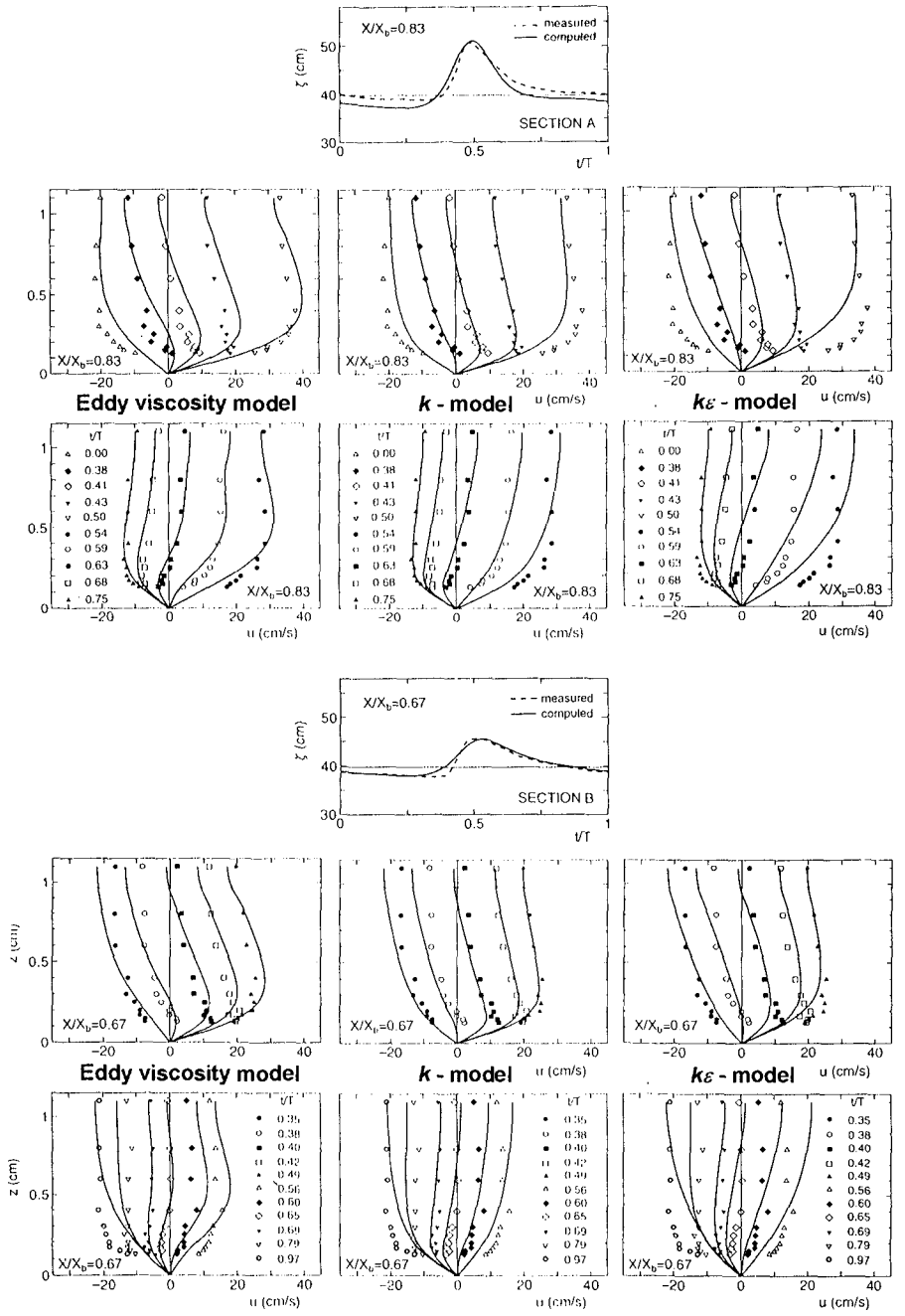


Figure 10. Comparison of vertical profiles of horizontal velocity inside the bottom boundary layer for the use of different distributions of the eddy viscosity.